molecules

MDPI

Article

Insight into the Binding Interaction between PEDCs and hERRγ Utilizing Molecular Docking and Molecular Dynamics Simulations

Fanqiang Bu [1,2], Lin Chen [1,*], Ying Sun [1], Bing Zhao [1,3] and Ruige Wang [1,*]

[1] College of Chemistry and Chemical Engineering, Qiqihar University, Qiqihar 161006, China; fanqiangbu@yeah.net (F.B.); m13895721559@163.com (Y.S.); 18304521342@163.com (B.Z.)
[2] State Key Laboratory of Organic-Inorganic Composites, Beijing Laboratory of Biomedical Materials, Beijing University of Chemical Technology, Beijing 100029, China
[3] Heilongjiang Provincial Key Laboratory of Surface Active Agent and Auxiliary, Qiqihar University, Qiqihar 161006, China
* Correspondence: chenlin201308@163.com (L.C.); wangrg716@163.com (R.W.)

Abstract: Phenolic environmental endocrine-disrupting chemicals (PEDCs) are persistent EDCs that are widely found in food packaging materials and environmental media and seriously threaten human health and ecological security. Human estrogen-related receptor γ (hERRγ) has been proposed as a mediator for the low-dose effects of many environmental PEDCs; however, the atomic-level descriptions of dynamical structural features and interactions of hERRγ and PEDCs are still unclarified. Herein, how three PEDCs, 4-(1-methylpropyl)phenol (4-sec-butylphenol), 5,6,7,8-tetrahydro-2-naphthol (tetrahydro-2-napthol), and 2,2-bis(4-hydroxy-3,5-dimethoxyphenyl)propane (BP(2,2)(Me)), interact with hERRγ to produce its estrogenic disruption effects was studied. Molecular docking and multiple molecular dynamics (MD) simulations were first conducted to distinguish the detailed interaction pattern of hERRγ with PEDCs. These binding structures revealed that residues around Leu271, Leu309, Leu345, and Phe435 are important when binding with PEDCs. Furthermore, the binding energies of PEDCs with hERRγ were also characterized using the molecular mechanics/Poisson Boltzmann surface area (MM-PBSA) and solvated interaction energy (SIE) methods, and the results showed that the interactions of CH-π, π-π, and hydrogen bonds are the major contributors for hERRγ binding to these three PEDCs. What is striking is that the methoxide groups of BP(2,2)(Me), as hydrophobic groups, can help to reduce the binding energy of PEDCs binding with hERRγ. These results provide important guidance for further understanding the influence of PEDCs on human health problems.

Keywords: hERRγ; PEDC; molecular docking; MD simulation; MM-PBSA; SIE

check for updates

Citation: Bu, F.; Chen, L.; Sun, Y.; Zhao, B.; Wang, R. Insight into the Binding Interaction between PEDCs and hERRγ Utilizing Molecular Docking and Molecular Dynamics Simulations. *Molecules* **2024**, *29*, 3256. https://doi.org/10.3390/molecules29143256

Academic Editor: Nino Russo

Received: 30 May 2024
Revised: 3 July 2024
Accepted: 3 July 2024
Published: 10 July 2024

Copyright: © 2024 by the authors. Licensee MDPI, Basel, Switzerland. This article is an open access article distributed under the terms and conditions of the Creative Commons Attribution (CC BY) license (https://creativecommons.org/licenses/by/4.0/).

1. Introduction

Environmental endocrine-disrupting chemicals (EDCs), which are widely found in food packaging materials and environmental media, can affect the synthesis, release, transmission, binding, and so on of hormones, resulting in biological developmental, reproductive, immune, neurological, or metabolic diseases in organisms [1–3]. Among them, phenolic EDCs (PEDCs) are toxic organic contaminants [4]. They have negative effects on the reproductive system, nervous system, and immune system of organisms, mainly intruding into the human body through the alimentary tract, respiratory system, and skin, binding to proteins in the cell protoplasm, and causing cell inactivation; they may even cause spinal cord stimulation, leading to systemic poisoning [5,6]. Therefore, many efforts have been made to investigate the effects of PEDCs on mammalian systems [7–9].

PEDCs can cause various health problems in organisms by affecting the normal functions of the reproductive, neural, and immune systems [10]. Estrogen-related receptors

(ERRs), a nuclear receptor transcription factor family [11], have three members, namely ERRα, ERRβ, and ERRγ, which act in various biologic processes such as cell energy metabolism [12]. ERRs mainly consist of an N-terminal transactivation domain, a central DNA-binding domain, and a C-terminal ligand-binding domain (LBD), as shown in Figure S1 [13]. The LBD consists of two antiparallel β-sheets (hereafter referred to as S1 and S2) and twelve α-helices (consisting of H1 to H12), and its hydrophobic binding pockets are composed of S1, S2, H3, H6, H7, H8, and H11. Human ERRγ (hERRγ), a constitutive active nuclear receptor, serves as a mediator for many low-dose effects of PEDCs. Through structural analysis, it was found that the majority of PEDCs in the external environment can bind in the pockets of hERRγ, thereby interfering with downstream signaling pathways [14]. Meanwhile, as hERRγ manages the expression of various disease-related genes, for example, those involved in cancer and adiposity, when its normal function is affected by exogenous compounds, the normal functioning of organisms could be severely affected [15–17]. Numerous studies have demonstrated that PEDCs can disrupt the normal functioning of nuclear receptors and also regulate the basic activity of hERRγ. Among these PEDCs, 4-sec-butylphenol and tetrahydro-2-napthol are important raw materials in many industrial products and are potential threats to people's health. Furthermore, BP(2,2)(Me), a sustainable bisphenol from lignin, is considered a promising alternative for commercial bisphenol [18]. A previous study by Thouennon et al. showed that the capacity of 4-sec-butylphenol and tetrahydro-2-napthol to bind with hERRγ is low, with EC_{50} values of approximately 109 and 260 nM, respectively [14]. Furthermore, Amitrano et al. revealed through molecular docking methods that the ability of BP(2,2)(Me) to bind with ERα is weak [18]. However, the atomic-level descriptions of the dynamical structural features and interactions of PEDCs with hERRγ are still unclarified. Therefore, exploring the mode of interaction between PEDCs and hERRγ is essential to uncovering the endocrine-disrupting mechanisms of PEDCs, which can help us to fully assess the latent diseases related to PEDC exposure.

Molecular docking is a popular approach used to predict the interactions between small ligands and the appropriate targets [19]. While there are a variety of docking programs in use, new computational methods based on artificial intelligence and machine learning are expected to make an even greater contribution [20–23]. In the past few decades, receptor–ligand interactions were broadly analyzed using traditional molecular dynamics (MD) simulations [24–27]. However, the conformations sampled by this approach may be swallowed in the locally minimal space, thereby resulting in under-sampling. As a valuable method, multiple MD simulations may preferably obtain the conformation of receptor–ligand interactions and can describe the dynamic and detailed interactions of receptors and ligands [28–33], which is a difficult task for experimental studies. Hence, in our work, the complexes of hERRγ with 4-sec-butylphenol, tetrahydro-2-napthol, and BP(2,2)(Me) (Figure 1) were taken as the research targets, and we explored the interaction mechanism between PEDCs and hERRγ using molecular docking, multiple MD simulations, and the MM-PBSA and SIE methods [34,35]. The dynamical structural features and interactions between hERRγ and PEDC were investigated, and the crucial residue distribution was assessed in our study. These results may offer new perspectives on the estrogen-disrupting effects of PEDCs.

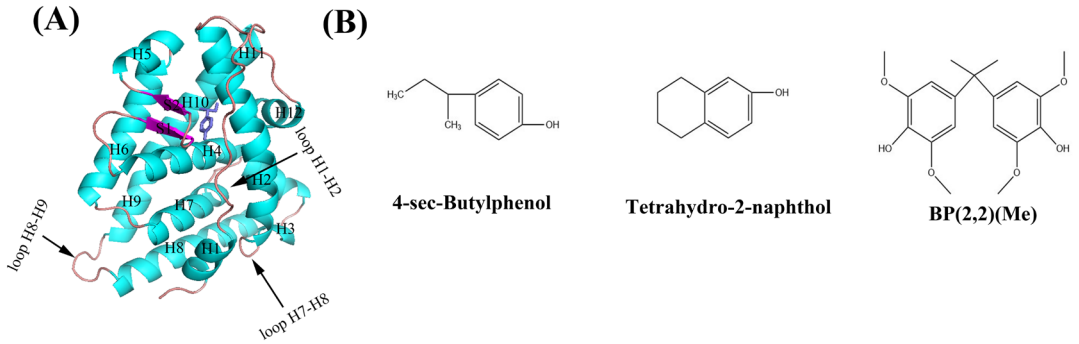


Figure 1. Structures of the complex of hERRγ with 4-sec-butylphenol ((**A**), PDB ID: 6I66) and the three PEDCs (**B**) in our study.

2. Results and Discussion

2.1. Dynamics of hERRγ-PEDC Complexes

To assess the stability of MD simulations of hERRγ-4-sec-butylphenol, hERRγ-tetrahydro-2-napthol, and hERRγ-BP(2,2)(Me) complexes, the root-mean-square deviations (RMSDs) for the hERRγ backbone atoms in MD simulations were evaluated compared with the corresponding original structure (Figure S2). After approximately 50 ns of simulations, the RMSD values in each hERRγ complex showed high stability. Therefore, the last 200 ns equilibrated portions of three replicas were connected, and each system possessed 600 ns trajectories for subsequent data analysis. The mean RMSD values of the hERRγ and 4-sec-butylphenol, tetrahydro-2-napthol, and BP(2,2)(Me) complexes were 2.31, 2.20, and 2.17 Å, respectively, indicating that the conformation of hERRγ in these complexes did not exhibit major structural change during the simulations. The experimental results of Thouennon et al. [14] also demonstrated the stability of hERRγ, as seen in the change in the hERRγ structure over time in Figure S3. In addition, to further evaluate the stability of the MD simulations, the enthalpy and entropy values were calculated (Figures S4 and S5). There were slight fluctuations in the calculated enthalpy and entropy between the different structures selected, but their cumulative average enthalpy and entropy values quickly stabilized. From the above analysis, it can be judged that the three complexes were stable in the 600 ns simulations. Therefore, post-processing analysis focused on these stable MD trajectories.

To investigate the detailed residual fluctuations in hERRγ interacting with different PEDCs, the root-mean-square fluctuations (RMSFs) in hERRγ Cα in the simulations related to the average coordinates of the joined 600 ns trajectory were computed. As shown in Figure S6, the flexibility patterns of residues in hERRγ were similar in these complexes. Among these complexes, residues near the active pockets composed of H2, H3, H5, H6, H10, S1, and S2 displayed a high degree of stability. This is mainly because the catalytic function of hERRγ requires a stable three-dimensional structure. However, the residues at both ends of hERRγ and around its loops showed high flexibility. It is worth noting that the residues around loops H1–H2, S1–S2, H7–H9, and H11–H12 exhibited distinct flexibility. In particular, loops such as S1–S2, H7–H8, and H10–H11 interacting with 4-sec-butylphenol and loop H1–H2 interacting with tetrahydro-2-naphthol showed high flexibility. The influence of environmental PEDCs on the internal dynamics of hERRγ was studied. This was performed using the ascertained correlated fluctuations in Cα (Figure S7). Obviously, in these complexes, the correlated motions of the D1 region, composed of H2 and H3–H4; the D2 region, composed of H2, s1, s2, and H5; the D3 region, composed of H7–H8 and H3–H4; the D4 region, composed of H5–H7 and H4–H5; the D5 region, composed of H10–H12 and H5–H6; and the D6 region, composed of H7–H8 and H8–H9, are more apparent. When hERRγ interacts with different PEDCs, the differences in its internal dynamics are the manifestation of changes in the relative position of residues in these complexes. The result is similar to the results of the RMSF analysis. In summary,

these structural changes may result in changes in the binding affinity between hERRγ and PEDCs.

2.2. Analysis of Free Energy between hERRγ and PEDCs

To gain insight into the source of energy differences in hERRγ with different PEDCs, the contributions of different energy terms were ascertained using the MM-PBSA approach (Table 1). Obviously, the calculated energies between hERRγ and 4-sec-butylphenol and between hERRγ and tetrahydro-2-napthol were −5.94 and −5.67 kcal/mol, respectively. These calculated energies have a good correlation with the experimental values for the hERRγ-4-sec-butylphenol (−9.49 kcal/mol) and hERRγ-tetrahydro-2-napthol (−8.98 kcal/mol) complexes [14]. When errors are taken into account, the energy results obtained are of the same order. In addition, the calculated energy of the hERRγ-BP(2,2)(Me) complex was −2.97 kcal/mol, which proves that BP(2,2)(Me) has weak interference ability on hERRγ; this is similar to the effect of BP(2,2)(Me) on ERα [18]. Nevertheless, the MM-PBSA method could not precisely reproduce the results from the experiment. The main factors include the following: (a) an explicit solvent was used in the MD simulation, while an implicit solvent was used in the MM-PBSA calculation [36]; (b) the intermediate electric constant (e) changes in the MD simulation, while the internal (e) is constant in the calculation with the MM-PBSA method [37]; and (c) there is less conformational entropy sampling in the MM-PBSA calculation [38,39]. In our work, we mainly performed the MM-PBSA method to calculate the discrepancies in the binding of PEDCs to hERRγ, rather than to reproduce the experimental results. Thus, the method is very suitable for calculating the energy of different EDCs for hERRγ. By comparing the separate energy components of these various complexes in Table 1, we observed that the chief driving force of hERRγ interacting with different PEDCs is van der Waals energy (ΔE_{vdW}) from nonpolar energy. The ΔE_{vdW} values between hERRγ and 4-sec-butylphenol, tetrahydro-2-napthol, and BP(2,2)(Me) were −23.95, −23.54, and −46.47 kcal/mol, respectively. In addition, in these complexes, electrostatic interaction energy (ΔE_{ele}) makes positive contributions to the binding of hERRγ with different PEDCs. The result conforms with the subsequent analysis of hydrogen bonds. However, polar solvation interactions destroy the interactions between different PEDCs and hERRγ, while nonpolar solvation interactions help them to interact. Moreover, the entropy (−TΔS) values of 4-sec-butylphenol, tetrahydro-2-napthol, and BP(2,2)(Me) with hERRγ were 15.21, 15.66, and 20.52 kcal/mol, respectively. These differences are mainly due to the vibrational entropy caused by structural changes when hERRγ interacts with different PEDCs.

Table 1. Binding free energy and its terms (kcal/mol) estimated via the MM-PBSA method.

System	hERRγ-4sec	hERRγ-2nap	hERRγ-BPMe
ΔE_{vdW}	−23.95 ± 2.28	−23.54 ± 2.20	−46.47 ± 2.64
ΔE_{ele}	−13.02 ± 3.29	−12.54 ± 6.15	−5.59 ± 4.66
$\Delta E_{(MM)}$	−36.97 ± 2.83	−36.08 ± 4.62	−52.06 ± 3.79
ΔG_{PB}	17.49 ± 2.98	16.30 ± 3.50	32.29 ± 4.45
ΔG_{SA}	−1.67 ± 0.08	−1.56 ± 0.09	−3.73 ± 0.12
ΔGsol	15.82 ± 2.11	14.74 ± 2.48	28.56 ± 3.15
ΔG_{polar}	4.47 ± 3.14	3.76 ± 5.00	26.70 ± 4.56
ΔG_{nonpol}	−25.62 ± 1.61	−25.10 ± 1.55	−50.20 ± 1.87
ΔH	−21.15 ± 3.29	−21.33 ± 3.82	−23.49 ± 3.79
−TΔS	15.21 ± 3.04	15.66 ± 3.10	20.52 ± 3.91
ΔG_{bind}	−5.94 ± 3.17	−5.67 ± 3.31	−2.97 ± 3.85
ΔG_{exp}	−9.49	−8.98	

Notes: Data are expressed as value ± standard deviation. $\Delta H = \Delta G_{polar} + \Delta G_{nonpol} = \Delta E_{ele} + \Delta G_{PB} + \Delta E_{vdW} + \Delta G_{SA}$. Experimental energy ($\Delta G_{exp}$) was calculated from inhibition constants (K_i) using $\Delta G_{exp} = RTlnK_i$.

To confirm the calculation results from the MM-PBSA method, the energies of hERRγ interacting with different PEDCs were also assessed based on the SIE approach (Table 2).

The free energies in hERRγ with 4-sec-butylphenol, tetrahydro-2-napthol, and BP(2,2)(Me) were −6.68, −6.54, and −5.68 kcal/mol, respectively. The results calculated using the SIE method agree well with the results from experiments [14,18]. The results of the above two energy calculations show that they can be used to study the interaction pattern of different PEDCs with hERRγ. As displayed in Table 2, in these PEDC and hERRγ complexes, the key interactions are the nonpolar interactions (ΔG_{nonpol}), including the ΔE_{vdW} and nonpolar contributions (ΔG_{cav}). Thus, the primary driving forces of the interactions between these PEDCs and hERRγ are hydrophobic interactions. Although the intermolecular Coulomb interactions (ΔE_{Coul}) are important for their binding, this effect is offset by the reaction energies (ΔG^{R}), which are between 4.17 and 9.96 kcal/mol. These energies (ΔG^{R}) are not conductive to the interaction of different PEDCs with hERRγ. ΔE_{Coul} also has a positive effect on PEDCs interacting with hERRγ. In light of the above MM-PBSA and SIE energy analyses, it can be seen that hydrophobic interactions composed of van der Waals energies are involved in the stability of PEDC and hERRγ complexes, which is also consistent with the results from the experiments [14,18].

Table 2. Binding free energy and its terms (kcal/mol) computed using the SIE method.

System	hERRγ-4sec	hERRγ-2nap	hERRγ-BPMe
ΔE_{vdW}	−27.63 ± 2.17	−25.93 ± 2.26	−28.37 ± 2.83
ΔE_{Coul}	−7.21 ± 1.42	−8.16 ± 2.74	−2.56 ± 2.37
ΔG_{cav}	−5.49 ± 0.24	−6.11 ± 0.27	−5.68 ± 0.61
ΔG^{R}	4.17 ± 0.74	5.34 ± 0.99	9.96 ± 1.69
ΔG_{nonpol}	−33.12 ± 1.13	−32.04 ± 1.61	−34.05 ± 2.06
ΔG_{pol}	−3.04 ± 1.54	−2.82 ± 1.94	7.4 ± 2.05
ΔG_{bind}	−6.68 ± 0.21	−6.54 ± 0.24	−5.68 ± 0.37
ΔG_{exp}	−9.49	−8.98	

Notes: Data are expressed as value ± standard deviation. $\Delta G_{pol} = \Delta G^{R} + \Delta E_{Coul}$, $\Delta G_{nonpol} = \Delta G_{cav} + \Delta E_{vdw}$. Experimental energy ($\Delta G_{exp}$) was calculated from inhibition constants (K_i) using $\Delta G_{exp} = RTlnK_i$.

2.3. Structure and Energy Relationship between hERRγ and PEDCs

To better understand the binding pattern of PEDCs and hERRγ, the hotspot residues of hERRγ when interacting with PEDCs were analyzed (Figure 2). Generally, the sources of important contributions to their interactions come from four regions around Leu271, Leu309, Leu345, and Phe435. It can be seen that the hydrophobic residues are important residues of the different PEDCs interacting with hERRγ, for example leucine. The experimental results almost agree with the dynamic structure analysis [14]. For example, residues Glu275 and Arg316 form hydrogen bonds with 4-sec-butylphenol. Phe435 also forms C-H/π interactions with 4-sec-butylphenol. Almost all of the important residues that interact with different PEDCs have weak polar interactions and strong nonpolar interactions, as shown in Tables S1–S3 and in Figure 3. Among the residues that interact with different PEDCs, except for residue Glu275, many of those involved in polar interactions form hydrogen bonds, as shown in Figure 4 and Table S4; those with small probabilities are not listed.

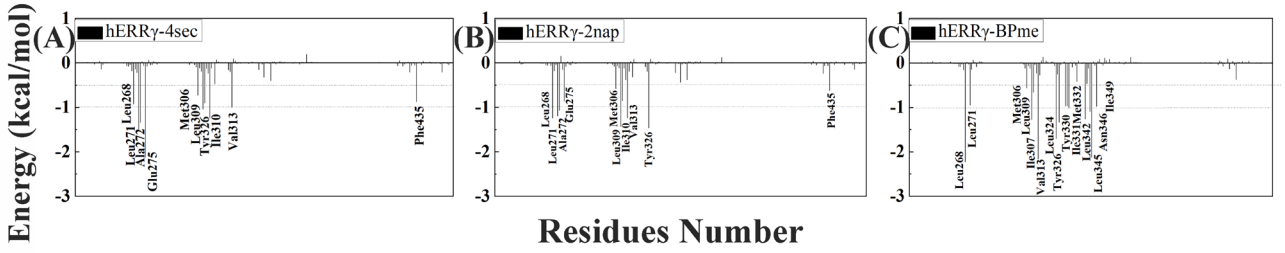


Figure 2. Contributions of key residues when interacting with different PEDCs: (**A**) 4-sec-butylphenol; (**B**) tetrahydro-2-napthol; (**C**) BP(2,2) (Me).

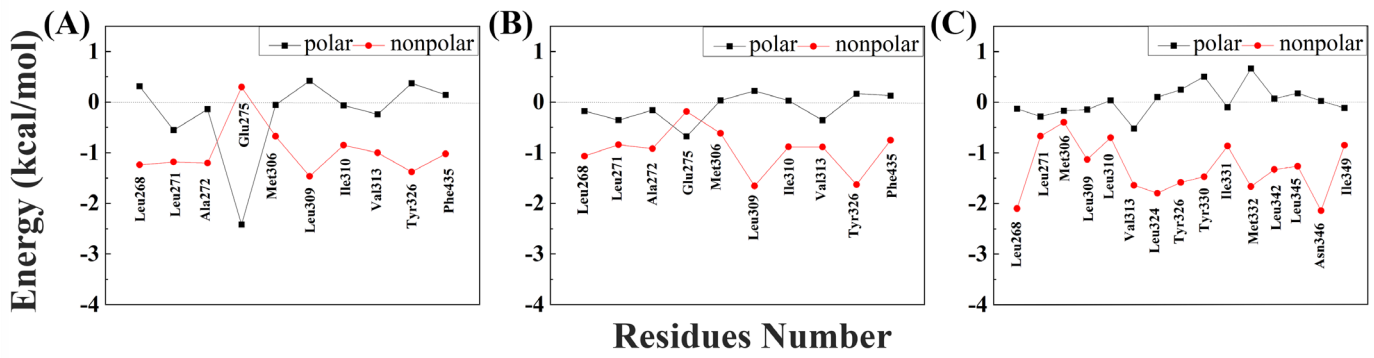


Figure 3. Nonpolar interaction and polar interaction energy of important residues when interacting with different PEDCs: (**A**) 4-sec-butylphenol; (**B**) tetrahydro-2-napthol; (**C**) BP(2,2)(Me).

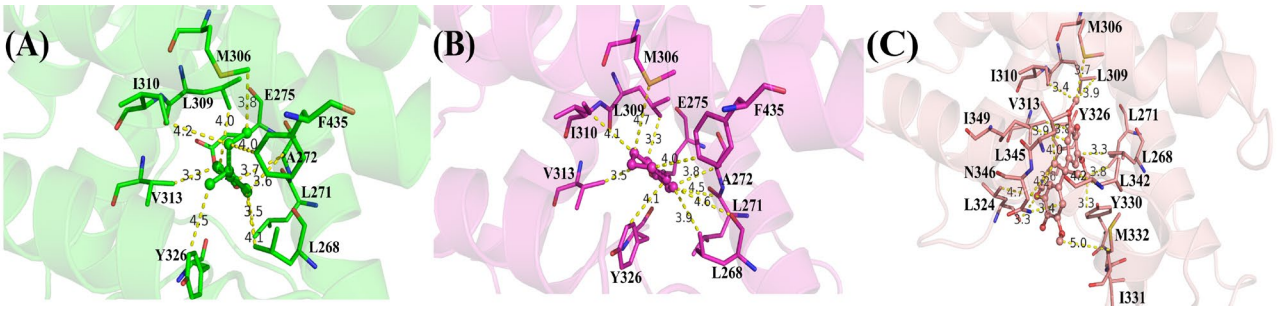


Figure 4. Interactions of different key residues when interacting with different PEDCs: (**A**) 4-sec-butylphenol (blue); (**B**) tetrahydro-2-napthol (magentas); (**C**) BP(2,2)(Me) (oranges).

For the hERRγ-4-sec-butylphenol complex, there were 10 residues with energies that contribute more than −0.5 kcal/mol (Figure 2A). Among these, the residues Leu271, Ala272, Glu275, Leu309, Val313, and Tyr326 provide over −1 kcal/mol of energy, which is important for interacting with 4-sec-butylphenol. Based on the nonpolar interactions (Figure 3A), the absolute values for the residues Leu268, Leu271, Ala272, Leu309, and Tyr326 exceeded −1 kcal/mol (Table S1). In this study of polar interactions, the absolute value of only one residue, Glu275, was more than 1 kcal/mol (Figure 3A); the spatial distribution is shown in Figure 4A. The energies between 4-sec-butylphenol and Leu268, Leu271, and Val313 are −0.92, −1.49, and −1.24 kcal/mol, respectively. This is mainly due to the interactions between the hydrophobic alkyls of these residues and the benzene group of 4-sec-butylphenol. The alkyl group of residue Ala272 is situated around the benzene ring of 4-sec-butylphenol, forming CH-π interactions. Thus, Ala272 binding with 4-sec-butylphenol contributes an energy value of −1.34 kcal/mol. The interaction of CH-HC between the side chain of Met306 and the alkyl of 4-sec-butylphenol is favorable for the interaction between hERRγ and 4-sec-butylphenol (−0.73 kcal/mol). The hydrophobic benzene ring of 4-sec-butylphenol can contact the isobutyl–methyl ring of Leu309 and the benzene ring of Tyr326 to form CH-π and T-shaped π-π, respectively. The results showed that residues Leu309 and Tyr326 contributed energies of nearly −1.04 and −1.00 kcal/mol, respectively. The electrostatic solvation interaction of residue Tyr326 is 0.37 kcal/mol, which impedes the interaction of hERRγ and 4-sec-butylphenol. In addition, the alkyl of Ile310 and the alkyl of 4-sec-butylphenol produce an energy of −0.91 kcal/mol. The van der Waals energy (−0.89 kcal/mol) for the hydrophobic group of Phe435 with the hydrophobic side chain of 4-sec-butylphenol is one of the key causes for the interaction between hERRγ and 4-sec-butylphenol (Figure 4A). Furthermore, Glu275 supplies −2.12 kcal/mol energy with 4-sec-butylphenol, primarily since the hydrogen bond occupancy of Glu275-OE1-H···OAC-4-sec-butylphenol is approximately 86.93% (Table S4).

For the hERRγ-tetrahydro-2-napthol complex, the energy contributions of 10 residues exceed −0.5 kcal/mol (Figure 2B); Leu268, Leu271, Ala272, Leu309, Val313, and Tyr326 offer

over −1 kcal/mol of energy. In our study of nonpolar interaction energies (Figure 3B), three residues, Leu268, Leu309, and Val313, possessed absolute values exceeding 1 kcal/mol (Table S2). The residues Met306, Ile310, and Val313, which closely resemble those for the hERRγ-4-sec-butylphenol complex, also contribute to a major interaction. The reason why these residues play a major role in hERRγ-tetrahydro-2-napthol is similar to that for the hERRγ-4-sec-butylphenol complex (Figure 4B). The difference is that the C-H···O interaction between the tetrahydro-2-napthol and carbonyl oxygen of Leu268 causes the backbone electrostatic energy of Leu268 to be −0.58 kcal/mol, so the total energy is increased by 0.32 kcal/mol. The alkyl of Leu271 is far away from the hydroxyl group of 4-sec-butylphenol, which is not conducive to the formation of CH-HO interactions. Therefore, the total contribution of Leu271 with tetrahydro-2-napthol is −1.19 kcal/mol. Compared with that in the hERRγ-4-sec-butylphenol complex, the energy of Ala272 with tetrahydro-2-napthol decreases by 0.27 kcal/mol. This results from the formation of a relatively weak interaction of the alkyl group of residue Ala272 with the hydrophobic benzene ring of tetrahydro-2-napthol. The interaction energy of Leu309 with tetrahydro-2-napthol increases by about 0.39 kcal/mol. This is connected with strengthened hydrophobic interactions of the alkyl ring of L309 with the benzene group of tetrahydro-2-napthol. Through comparison with the hERRγ-4-sec-butylphenol complex, we see that the binding pattern of tetrahydro-2-napthol with hERRγ resembles that of 4-sec-butylphenol with hERRγ, and the van der Waals energies (−1.47 and −0.63 kcal/mol) between the alkyls of residues Tyr326 and Phe435 and the hydrophobic benzene ring of tetrahydro-2-napthol are also a significant reason for their binding.

When hERRγ interacts with BP(2,2)(Me), there are 15 residues with energy over −0.5 kcal/mol (Figure 2C). Importantly, Leu268, Leu309, Val313, Leu324, Tyr326, Met332, Leu342, Leu345, and Asn346 make the largest contribution to BP(2,2)(Me), with amounts above −1 kcal/mol. As shown in this study of their nonpolar interaction energy (Figure 3C), the absolute values of the energy of nine residues, Leu268, Leu309, Val313, Leu324, Tyr326, Tyr330, Met33, Leu342, Leu345, and Asn346, are all over −1 kcal/mol (Table S3), and the spatial distribution of these important residues is depicted in Figure 4C. Nevertheless, nearly all of the primary residues binding to BP(2,2)(Me) have weak polar interactions. The energy of residue Leu268 in hERRγ-BP(2,2)(Me) bears a resemblance to that in the hERRγ-4-sec-butylphenol complex, playing an essential interaction role similar to that in hERRγ-4-sec-butylphenol. Leu309, Val313, Tyr326, Tyr330, and Ile331 have enhanced interactions with BP(2,2)(Me) compared with those in hERRγ-4-sec-butylphenol, which is related to enhanced interactions forming alkyl rings with the methoxy group of BP(2,2)(Me). Differently, the interactions of Leu271, Met306, and Ile310 with BP(2,2)(Me) are weakened. CO-H interactions were found for the carbonyl oxygen of Leu324 with the hydrophobic methoxy group of BP(2,2)(Me); therefore, electrostatic energy (−0.86 kcal/mol) is the primary interacting force. The interactions of Leu342 and Leu345 with BP(2,2)(Me) are also reinforced. They are associated with the enhanced interactions forming alkyl rings of these residues and alkyl groups of BP(2,2)(Me). Additionally, the hydrophobic alkyl group of Ile349 is located near the benzene ring of BP(2,2)(Me), forming a CH-π interaction. Thus, residue Ile349 offers approximately −0.97 kcal/mol to the interaction with BP(2,2)(Me).

On the whole, the binding of various PEDCs causes changes in their local structure by influencing the interactions with various residues. The most representative structural superimposition (Figures S8 and S9) demonstrates the significant change in loops H1-H2, H7-H8, and H8-H9. However, residues around Leu268, Val313, Leu345, and Phe435 can interact stably with various PEDCs, and CH-π, π-π, and hydrogen bond interactions between these PEDCs and important residues in hERRγ are the key to the stable existence of these complexes.

3. Materials and Methods

3.1. Molecular Docking

Two structures of hERRγ-4-sec-butylphenol and hERRγ-tetrahydro-2-napthol were obtained from RCSB (PDB ID: 6I66 and 6I67) [14]. Since there was no complex structure of hERRγ and BP(2,2)(Me), AutoDock 4.2 software [40] was used to dock BP(2,2)(Me) to the binding site of hERRγ. BP(2,2)(Me) was first optimized with the B3LYP method under the 6–31 g(d) basis set of the Gaussian09 package [41]. During docking, the coordinates of hERRγ were obtained by removing all crystal water and ligands based on the hERRγ-4-sec-butylphenol complex. The binding site of hERRγ with 4-sec-butylphenol was considered as the binding pocket for docking. Firstly, 4-sec-butylphenol was redocked with hERRγ to affirm the reliability of the docking method. After superimposing the experimental and docking structures, the conformation of the two structures was basically the same (Figure S10), indicating that the docking method was credible. Then, docking between BP(2,2)(Me) and hERRγ was performed using the graphical user interface of Auto Dock Tools. The semi-flexible docking method was performed to maintain the rigidity of hERRγ while allowing for the flexibility of the ligand. The grid box was set based on the binding pocket of the 4-sec-butylphenol ligand. The grid center coordinates of hERRγ in the X, Y, and Z directions were −15.03, −3.06, and −24.24, respectively. The size was set to 44 Å × 44 Å × 38 Å with a grid point spacing of 0.375 Å. The Lamarckian genetic algorithm was used for docking. One hundred optimal conformations were obtained for each hERRγ and PEDC docking result through the iterative search process. In the end, the complex with the lowest energy was retained for further analysis.

3.2. System Setup

Owing to the lack of parameters needed for the ligands 4-sec-butylphenol, tetrahydro-2-napthol, and BP(2,2)(Me) in the force field, optimization of these ligands was first conducted based on the Gaussian package. The missing hydrogen atoms were added to the corresponding heavy atoms of each system by applying the tLeap program in Amber 18 [42]. A standard amber (ff14SB) force field [43] was chosen to depict hERRγ, while a general amber force field [44] with AM1-BCC charges was employed to set the three PEDCs' parameters. A truncated octahedral periodic box filled with TIP3P water [45] was used to process these systems. The distance forming the outermost atoms with the water box was over 12 Å. Generally, each system included more than 12,000 water molecules. In addition, to neutralize each simulated system, TIP3P water molecules were replaced with Na^+.

3.3. MD Simulation

Prior to the MD simulations, to eliminate possible bad contact, each system was energetically minimized with complex atoms with force constants of 50 kcal mol^{-1} $Å^{-2}$ through 4000 steepest descent steps and another 8000 conjugate gradient steps. Following that, canonical ensemble MD simulation was conducted for 600 ps, during which each system was heated progressively to 310 K at a constant force of 10 kcal mol^{-1} $Å^{-2}$. Afterwards, an isothermal isobaric ensemble MD simulation for 1000 ps was applied with the complex atoms constrained. Ultimately, for each system under the *NPT* ensemble, three 250 ns simulations were performed. According to the Maxwell distribution, seeds with different values were randomly distributed to each repeated system. Long-range electrostatic interactions were calculated using the particle mesh Ewald method [46] with default values. The SHAKE algorithm [47] was constrained to bonds communicating with hydrogen atoms. The time step was 2 fs. Unless otherwise specified, the data in the figures and tables were analyzed based on connected 600 ns trajectories. PyMOL2.0 soft [48] was mainly conducted to imagine the trajectory and to portray structures. The MD simulations, including the energy minimization, were conducted using Amber18 soft with GPU-accelerated PMEMD [42].

3.4. MM-PBSA Calculation

The MM-PBSA method [49–53] implemented in amber18 was executed to calculate the binding free energy (ΔG_{bind}) for the hERRγ-4-sec-butylphenol, hERRγ-tetrahydro-2-napthol, and hERRγ-BP(2,2)(Me) complexes. The energy was the values computed for 3000 structure samplings based on the equilibrated portions at 200 ps intervals. The calculation formulas are presented as follows:

$$\Delta G_{bind} = G_{complex} - G_{receptor} - G_{ligand} \quad (1)$$

$$\Delta G_{bind} = \Delta H - T\Delta S \quad (2)$$

$$\Delta H = \Delta E_{ele} + \Delta E_{vdW} + \Delta G_{PB} + \Delta G_{SA} \quad (3)$$

$$\Delta G_{SA} = \gamma \Delta SASA + \beta \quad (4)$$

ΔE_{ele}, ΔE_{vdW}, ΔG_{PB}, and ΔG_{SA} represent the energies of electrostatic interaction, van der Waals interaction, polar solvation, and nonpolar solvation, respectively. ΔG_{PB} and ΔG_{SA} were estimated using the PB model and ΔSASA, respectively. The two empirical constants γ and β were 0.00542 kcal mol^{-1} Å^{-2} and 0.92 kcal mol^{-1}, respectively. The ionic strength was 0.1 M, and the dielectric constants were 1.0 and 80.0 for the solute and surrounding solvent, respectively [54]. The entropy ($T\Delta S$) was calculated via Normal-mode analysis [55] with the nmode module. Since the entropy calculation was expensive, only 100 structures based on 3000 structures were selected for calculation.

3.5. SIE Calculation

The SIE method [34,35,56] was performed to estimate the energy for the hERRγ-4-sec-butylphenol, hERRγ-tetrahydro-2-napthol, and hERRγ-BP(2,2)(Me) complexes. The calculation formulas are as follows:

$$\Delta G_{bind}(\rho, D_{in}, \alpha, \gamma, C) = \alpha[E_{Coul}(D_{in}) + E_{vdw} + \Delta G_R(\rho, D_{in}) + G_{cav}(\rho) + C] \quad (5)$$

$$G_{cav} = \gamma \Delta M_{SA} \quad (6)$$

E_{Coul}, E_{vdW}, ΔG^R, and G_{cav} describe the intermolecular Coulomb, van der Waals, reaction, and nonpolar solvation energy, respectively. ΔG^R and G_{cav} were estimated using the boundary element method and ΔM_{SA}, respectively.

The three empirical constants ρ, D_{in}, and α represent the linear scaling factor of van der Waals radii and the internal dielectric invariable of the solute, respectively. The values of ρ, D_{in}, α, γ, and C were 1.1, 2.25, 0.1048, 0.0129 kcal mol^{-1} Å^{-2}, and −2.89 kcal mol^{-1}, respectively. When calculating the energy using the Sietraj program for SIE calculations [34], the same 3000 structures as in the MM-PBSA calculation were chosen.

3.6. Conformational Dynamics Analysis

Based on the uniform sampling of equilibrium trajectories, the cross-correlation matrix [57] was calculated. The fluctuation of Cα atoms compared with their average positions in hERRγ during the simulation was used to assess the cross-correlation coefficient (C_{ij}). The formula is as follows:

$$C_{ij} = \frac{< \Delta r_i \Delta r_j >}{\left(< \Delta r_i^2 >< \Delta r_j^2 > \right)^2} \quad (7)$$

The symbol Δr_i describes the displacement of the i-th atom from the mean position. The value of C_{ij} is between −1 and 1. A positive C_{ij} value shows positively correlated movement, while a negative C_{ij} value shows negatively correlated movement.

3.7. Principal Component Analysis

To describe the collective motions of hERRγ during the simulation period, principal component analysis (PCA) [58–60] was conducted using ProDy2.0 software [61]. On

the basis of uniform sampling of the equilibrium trajectory, the covariance matrix of the diagonal coordinate system was constructed through PCA. The movement analysis steps of hERRγ were, first, to project the trajectory in the direction described through the corresponding eigenvector and, second, to determine the main motion direction of hERRγ according to the first two eigenvalues. Through VMD 1.9.3 [62] software with the NMWiz plug-in, the 3D structure of hERRγ was visualized.

4. Conclusions

Molecular docking and MD simulations were executed to probe the conformational changes and interactions in hERRγ complexes with three PEDCs (4-sec-butylphenol, tetrahydro-2-napthol, and BP(2,2)(Me)). Furthermore, two energy computation methods (MM-PBSA and SIE) were used to uncover the important residues between them.

The docking and simulation results demonstrated that when these three PEDCs interact with hERRγ, residues near Leu268, Val313, Leu345, and Phe435 play significant roles in their interactions. Moreover, the energy analysis indicated that hydrophobic interactions resulting from van der Waals energies are involved in the stability of the binding between these three PEDCs and hERRγ, which is crucial in their interaction. In addition, the interactions of CH-π, π-π, and hydrogen bonds are major contributors to hERRγ binding to these three PEDCs. What is striking is that the hydrophobic methoxide groups of BP(2,2)(Me) can help to reduce the binding energy of PEDCs with hERRγ.

These findings clarify the details of these three PEDCs binding to hERRγ, which can provide estimable knowledge for further understanding of the influence of PEDCs on human health problems.

Supplementary Materials: The following supporting information can be downloaded at: https://www.mdpi.com/article/10.3390/molecules29143256/s1, Tables S1–S3. Different energy components of important residues. Table S4. Important hydrogen bonds between PEDCs and hERRγ. Figure S1. The structural domains of ERRs. Figure S2. Time series of RMSDs. Figure S3. hERRγ secondary structure evolution. Figures S4–S5. Change in enthalpies and entropies and cumulative mean values. Figure S6. RMSF values of Cα atoms. Figure S7. Cross-correlation matrices. Figure S8. PC1 mode for hERRγ. Figure S9. Representative conformation superimposition. Figure S10. Structural superimposition.

Author Contributions: Investigation, data curation, and writing—original draft preparation, F.B. and Y.S.; investigation, B.Z.; methodology, investigation, and writing—review and editing, L.C. and R.W. All authors have read and agreed to the published version of the manuscript.

Funding: This research was funded by [Heilongjiang Educational Committee], grant number [145209504].

Institutional Review Board Statement: Not applicable.

Informed Consent Statement: Not applicable.

Data Availability Statement: The data used to support the findings of this study are included in the article.

Acknowledgments: The authors acknowledge financial assistance from The Fundamental Research Funds for Heilongjiang Educational Committee (145209504).

Conflicts of Interest: The authors declare no conflicts of interest.

References

1. Wan, M.L.Y.; Co, V.A.; El-Nezami, H. Endocrine disrupting chemicals and breast cancer: A systematic review of epidemiological studies. *Crit. Rev. Food Sci. Nutr.* **2022**, *62*, 6549–6576. [CrossRef]
2. Ismanto, A.; Hadibarata, T.; Kristanti, R.A.; Maslukah, L.; Safinatunnajah, N.; Kusumastuti, W. Endocrine disrupting chemicals (EDCs) in environmental matrices: Occurrence, fate, health impact, physio-chemical and bioremediation technology. *Environ. Pollut.* **2022**, *302*, 119061. [CrossRef]

3. Kouiti, M.; Castillo-Hermoso, M.Á.; Youlyouz-Marfak, I.; Khan, K.S.; Thangaratinam, S.; Olmedo-Requena, R.; Zamora, J.; Jiménez-Moléon, J.J. Persistent organic pollutant exposure as a risk factor of gestational diabetes mellitus: A systematic review and meta-analysis. *BJOG-Int. J. Obstet. Gy.* **2024**, *131*, 579–588. [CrossRef]
4. Sieck, N.E.; Bruening, M.; van Woerden, I.; Whisner, C.; Payne-Sturges, D.C. Effects of Behavioral, Clinical, and Policy Interventions in Reducing Human Exposure to Bisphenols and Phthalates: A Scoping Review. *Environ. Health Perspect.* **2024**, *132*, 36001. [CrossRef]
5. Pan, Z.; Tang, C.; Cao, Y.; Xuan, Y.; Zhou, Q. Distribution and source apportionment of phenolic EDCs in rivers in the Pearl River Delta, South China. *Environ. Sci. Pollut. Res.* **2023**, *30*, 48248–48259. [CrossRef]
6. Otitoju, O.B.; Alfred, M.O.; Ogunlaja, O.O.; Olorunnisola, C.G.; Olukanni, O.D.; Ogunlaja, A.; Omorogie, M.O.; Unuabonah, E.I. Pollution and risk assessment of phenolic compounds in drinking water sources from South-Western Nigeria. *Environ. Sci. Pollut. Res.* **2023**, *30*, 76798–76817. [CrossRef]
7. Xu, R.; Liu, S.; Pan, Y.-F.; Wu, N.-N.; Huang, Q.-Y.; Li, H.-X.; Lin, L.; Hou, R.; Xu, X.-R.; Cheng, Y.-Y. Steroid metabolites as overlooked emerging contaminants: Insights from multimedia partitioning and source–sink simulation in an estuarine environment. *J. Hazard. Mater.* **2024**, *461*, 132673. [CrossRef]
8. Ibor, O.R.; Nnadozie, P.; Ogarekpe, D.M.; Idogho, O.; Anyanti, J.; Aizobu, D.; Onyezobi, C.; Chukwuka, A.V.; Adeogun, A.O.; Arukwe, A. Public health implications of endocrine disrupting chemicals in drinking water and aquatic food resources in Nigeria: A state-of-the-science review. *Sci. Total. Environ.* **2023**, *858*, 159835. [CrossRef]
9. Zhang, C.; Lu, J.; Wu, J. Enhanced removal of phenolic endocrine disrupting chemicals from coastal waters by intertidal macroalgae. *J. Hazard. Mater.* **2021**, *411*, 125105. [CrossRef]
10. Alizada, S.; Eminli, F.; Vakhshouri, A.R. A review of novel electrode materials and techniques for electro-Fenton process applied to the degradation of phenolic compounds. *Water Environ. J.* **2023**, *37*, 390–401. [CrossRef]
11. Cavallini, A.; Notarnicola, M.; Giannini, R.; Montemurro, S.; Lorusso, D.; Visconti, A.; Minervini, F.; Caruso, M.G. Oestrogen receptor-related receptor alpha (ERRα) and oestrogen receptors (ERα and ERβ) exhibit different gene expression in human colorectal tumour progression. *Eur. J. Cancer* **2005**, *41*, 1487–1494. [CrossRef] [PubMed]
12. Ouyang, X.; Zhu, X.; Wang, L.; Zheng, X.; Wang, J. Effect of bisphenol A on the ovarian expressions of estrogen-related receptor gene and protein in queen honey bee (Apis mellifera). *Apidologie* **2023**, *54*, 60. [CrossRef]
13. Chen, L.; Lin, X.; Shi, S.; Li, M.; Mortimer, M.; Fang, W.; Li, F.; Guo, L.-H. Activation of estrogen-related receptor: An alternative mechanism of hexafluoropropylene oxide homologs estrogenic effects. *Sci. Total. Environ.* **2023**, *901*, 166257. [CrossRef] [PubMed]
14. Thouennon, E.; Delfosse, V.; Bailly, R.; Blanc, P.; Boulahtouf, A.; Grimaldi, M.; Barducci, A.; Bourguet, W.; Balaguer, P. Insights into the activation mechanism of human estrogen-related receptor γ by environmental endocrine disruptors. *Cell. Mol. Life Sci.* **2019**, *76*, 4769–4781. [CrossRef] [PubMed]
15. Sangwan, S.; Bhattacharyya, R.; Banerjee, D. Plastic compounds and liver diseases: Whether bisphenol A is the only culprit. *Liver Int.* **2024**, *44*, 1093–1105. [CrossRef] [PubMed]
16. Madhavan, S.; Gusev, Y.; Singh, S.; Riggins, R.B. ERRγ target genes are poor prognostic factors in Tamoxifen-treated breast cancer. *J. Exp. Clin. Cancer Res.* **2015**, *34*, 45. [CrossRef] [PubMed]
17. Lasheras, J.; Pardo, R.; Velilla, M.; Poncelas, M.; Salvatella, N.; Simó, R.; Ruiz-Meana, M.; Zamora, M.; Villena, J.A. Cardiac-Specific Overexpression of ERRγ in Mice Induces Severe Heart Dysfunction and Early Lethality. *Int. J. Mol. Sci.* **2021**, *22*, 8047. [CrossRef] [PubMed]
18. Amitrano, A.; Mahajan, J.S.; Korley, L.T.J.; Epps, T.H. Estrogenic activity of lignin-derivable alternatives to bisphenol A assessed via molecular docking simulations. *RSC Adv.* **2021**, *11*, 22149–22158. [CrossRef] [PubMed]
19. Muhammed, M.T.; Aki-Yalcin, E. Molecular docking: Principles, advances, and its applications in drug discovery. *Lett. Drug. Des. Discov.* **2024**, *21*, 480–495. [CrossRef]
20. Shanker, S.; Sanner, M.F. Predicting Protein–Peptide Interactions: Benchmarking Deep Learning Techniques and a Comparison with Focused Docking. *J. Chem. Inf. Model.* **2023**, *63*, 3158–3170. [CrossRef]
21. Vitali, E.; Ficarelli, F.; Bisson, M.; Gadioli, D.; Accordi, G.; Fatica, M.; Beccari, A.R.; Palermo, G. GPU-optimized approaches to molecular docking-based virtual screening in drug discovery: A comparative analysis. *J. Parallel Distrib. Comput.* **2024**, *186*, 104819. [CrossRef]
22. Yasir, M.; Park, J.; Han, E.-T.; Park, W.S.; Han, J.-H.; Kwon, Y.-S.; Lee, H.-J.; Chun, W. Machine Learning-Based Drug Repositioning of Novel Janus Kinase 2 Inhibitors Utilizing Molecular Docking and Molecular Dynamic Simulation. *J. Chem. Inf. Model.* **2023**, *63*, 6487–6500. [CrossRef] [PubMed]
23. Yanagisawa, K.; Fujie, T.; Takabatake, K.; Akiyama, Y. QUBO Problem Formulation of Fragment-Based Protein–Ligand Flexible Docking. *Entropy* **2024**, *26*, 397. [CrossRef] [PubMed]
24. Xue, Q.; Liu, X.; Liu, X.-C.; Pan, W.-X.; Fu, J.-J.; Zhang, A.-Q. The Effect of Structural Diversity on Ligand Specificity and Resulting Signaling Differences of Estrogen Receptor α. *Chem. Res. Toxicol.* **2019**, *32*, 1002–1013. [CrossRef] [PubMed]
25. Li, L.; Wang, Q.; Zhang, Y.; Niu, Y.; Yao, X.; Liu, H. The Molecular Mechanism of Bisphenol A (BPA) as an Endocrine Disruptor by Interacting with Nuclear Receptors: Insights from Molecular Dynamics (MD) Simulations. *PLoS ONE* **2015**, *10*, e0120330. [CrossRef] [PubMed]
26. Xue, W.; Liu, H.; Yao, X. Molecular mechanism of hiv-1 integrase-vdna interactions and strand transfer inhibitor action: A molecular modeling perspective. *J. Comput. Chem.* **2012**, *33*, 527–536. [CrossRef] [PubMed]

27. Na, L.; Zhou, W.; Yue, G.; Wang, J.; Fu, W.; Sun, H.; Li, D.; Duan, M.; Hou, T. Molecular dynamics simulations revealed the regulation of ligands to the interactions between androgen receptor and its coactivator. *J. Chem. Inf. Model.* **2018**, *58*, 1652–1661.
28. Auffinger, P.; Westhof, E. Rna hydration: Three nanoseconds of multiple molecular dynamics simulations of the solvated trnaasp anticodon hairpin. *J. Mol. Biol.* **1997**, *269*, 326–341. [CrossRef] [PubMed]
29. Caves, L.S.D.; Evanseck, J.D.; Karplus, M. Locally accessible conformations of proteins: Multiple molecular dynamics simulations of crambin. *Protein Sci.* **2010**, *7*, 7649–7666. [CrossRef]
30. Chen, L.; Huang, X.; Li, Y.; Zhao, B.; Liang, M.; Wang, R. Structural and energetic basis of interaction between human estrogen-related receptor γ and environmental endocrine disruptors from multiple molecular dynamics simulations and free energy predictions. *J. Hazard. Mater.* **2023**, *443*, 130174. [CrossRef]
31. Knapp, B.; Ospina, L.; Deane, C.M. Avoiding False Positive Conclusions in Molecular Simulation: The Importance of Replicas. *J. Chem. Theory Comput.* **2018**, *14*, 6127–6138. [CrossRef]
32. Wang, L.; Lu, D.; Wang, Y.; Xu, X.; Zhong, P.; Yang, Z. Binding selectivity-dependent molecular mechanism of inhibitors towards CDK2 and CDK6 investigated by multiple short molecular dynamics and free energy landscapes. *J. Enzym. Inhib. Med. Chem.* **2023**, *38*, 84–99. [CrossRef]
33. Wang, R.; Zheng, Q. Multiple Molecular Dynamics Simulations and Energy Analysis Unravel the Dynamic Properties and Binding Mechanism of Mutants HIV-1 Protease with DRV and CA-p2. *Microbiol. Spectr.* **2022**, *10*, e0074821. [CrossRef] [PubMed]
34. Sulea, T.; Cui, Q.; Purisima, E.O. Solvated interaction energy (SIE) for scoring protein–ligand binding affinities. 2. Benchmark in the CSAR-2010 scoring exercise. *J. Chem. Inf. Model.* **2011**, *51*, 2066–2081. [CrossRef]
35. Naïm, M.; Bhat, S.; Rankin, K.; Dennis, S.; Chowdhury, S.; Siddiqi, I.; Drabik, P.; Sulea, T.; Bayly, C.; Jakalian, A.; et al. Solvated interaction energy (SIE) for scoring protein−ligand binding affinities. 1. Exploring the parameter space. *J. Chem. Inf. Model.* **2007**, *47*, 122–133. [CrossRef]
36. Huang, K.; Luo, S.; Cong, Y.; Zhong, S.; Zhang, J.Z.; Duan, L. An accurate free energy estimator: Based on MM/PBSA combined with interaction entropy for protein–ligand binding affinity. *Nanoscale* **2020**, *12*, 10737–10750. [CrossRef]
37. Ravindranathan, K.; Tirado-Rives, J.; Jorgensen, W.L.; Guimarães, C.R.W. Improving MM-GB/SA Scoring through the Application of the Variable Dielectric Model. *J. Chem. Theory Comput.* **2011**, *7*, 3859–3865. [CrossRef] [PubMed]
38. Srinivasan, J.; Cheatham, T.E.; Cieplak, P.; Kollman, P.A.; Case, D.A. Continuum Solvent Studies of the Stability of DNA, RNA, and Phosphoramidate—DNA Helices. *J. Am. Chem. Soc.* **1998**, *120*, 9401–9409. [CrossRef]
39. Gohlke, H.; Case, D.A. Converging free energy estimates: MM-PB (GB) SA studies on the protein–protein complex Ras–Raf. *J. Comput. Chem.* **2004**, *25*, 238–250. [CrossRef]
40. Morris, G.M.; Huey, R.; Lindstrom, W.; Sanner, M.F.; Belew, R.K.; Goodsell, D.S.; Olson, A.J. AutoDock4 and AutoDockTools4: Automated docking with selective receptor flexibility. *J. Comput. Chem.* **2009**, *30*, 2785–2791. [CrossRef]
41. Frisch, M.J.; Trucks, G.W.; Schlegel, H.B.; Scuserica, G.E.; Robb, M.A.; Cheeseman, J.R.; Scalmani, G.; Barone, V.; Mennucci, B.; Petersson, G.A.; et al. *Gaussian 09*; Gaussian, Inc.: Wallingford, CT, USA, 2009.
42. Case, D.A.; Cheatham, T.E., III; Darden, T.A.; Glhike, H.; Luo, R.; Merz, K.M.; Onufriev, A.; Simmerling, C.L.; Wang, B.; Woods, R.J. The Amber biomolecular simualtion programs. *J. Comput. Chem.* **2005**, *26*, 1668–1688. [CrossRef]
43. Maier, J.A.; Martinez, C.; Kasavajhala, K.; Wickstrom, L.; Hauser, K.E.; Simmerling, C. ff14SB: Improving the accuracy of protein side chain and backbone parameters from ff99SB. *J. Chem. Theory Comput.* **2015**, *11*, 3696–3713. [CrossRef] [PubMed]
44. Wang, J.; Wolf, R.M.; Caldwell, J.W.; Kollman, P.A.; Case, D.A. Development and testing of a general amber force field. *J. Comput. Chem.* **2004**, *25*, 1157–1174. [CrossRef]
45. Jorgensen, W.L.; Chandrasekhar, J.; Madura, J.D.; Impey, R.W.; Klein, M.L. Comparison of simple potential functions for simulating liquid water. *J. Chem. Phys.* **1983**, *79*, 926–935. [CrossRef]
46. Darden, T.; York, D.; Pedersen, L. Particle mesh Ewald: An N.log (N) method for Ewald sums in large systems. *J. Comput. Phys.* **1993**, *98*, 10089–10092. [CrossRef]
47. KrUtler, V.; Gunsteren, W.F.V.; Hünenberger, H.P. A fast shake algorithm to solve distance constraint equations for small molecules in molecular dynamics simulations. *J. Comput. Chem.* **2015**, *22*, 501–508. [CrossRef]
48. DeLano, W.L. Pymol: An open-source molecular graphics tool. *CCP4 Newsl. Protein Crystallogr* **2002**, *40*, 82–92.
49. Hou, T.; Wang, J.; Wang, Y.; Li, W. Assessing the performance of the MM/PBSA and MM/GBSA methods. 1. The accuracy of binding free energy calculations based on molecular dynamics simulations. *J. Chem. Inf. Model.* **2011**, *51*, 69–82. [CrossRef]
50. Sun, H.; Li, Y.; Tian, S.; Xu, L.; Hou, T. Assessing the performance of MM/PBSA and MM/GBSA methods. 4. Accuracies of MM/PBSA and MM/GBSA methodologies evaluated by various simulation protocols using PDB bind data set. *Phys. Chem. Chem. Phys.* **2014**, *16*, 16719–16729. [CrossRef] [PubMed]
51. Swanson, J.M.; Henchman, R.H.; McCammon, J.A. Revisiting Free Energy Calculations: A Theoretical Connection to MM/PBSA and Direct Calculation of the Association Free Energy. *Biophys. J.* **2004**, *86*, 67–74. [CrossRef] [PubMed]
52. Luo, R.; David, L.; Gilson, M.K. Accelerated Poisson–Boltzmann calculations for static and dynamic systems. *J. Comput. Chem.* **2002**, *23*, 1244–1253. [CrossRef]
53. Genheden, S.; Ryde, U. The MM/PBSA and MM/GBSA methods to estimate ligand-binding affinities. *Expert Opin. Drug Discov.* **2015**, *10*, 449–461. [CrossRef]

54. Sun, H.; Li, Y.; Shen, M.; Tian, S.; Xu, L.; Pan, P.; Guan, Y.; Hou, T. Assessing the performance of MM/PBSA and MM/GBSA methods. 5. Improved docking performance using high solute dielectric constant MM/GBSA and MM/PBSA rescoring. *Phys. Chem. Chem. Phys.* **2014**, *16*, 22035–22045. [CrossRef] [PubMed]
55. Case, D.A. Normal mode analysis of protein dynamics. *Curr. Opin. Struct. Biol.* **1994**, *4*, 285–290. [CrossRef]
56. Cui, Q.; Sulea, T.; Schrag, J.D.; Munger, C.; Hung, M.N.; Naïm, M.; Cygler, M.E.; Purisima, O. Molecular dynamics-Solvated interaction energy studies of protein–protein interactions: The MP1–p14 scaffolding complex. *J. Mol. Biol.* **2008**, *379*, 787–802. [CrossRef] [PubMed]
57. Hünenberger, P.; Mark, A.; van Gunsteren, W. Fluctuation and Cross-correlation Analysis of Protein Motions Observed in Nanosecond Molecular Dynamics Simulations. *J. Mol. Biol.* **1995**, *252*, 492–503. [CrossRef] [PubMed]
58. Balsera, M.A.; Wriggers, W.; Oono, Y.; Schulten, K. Principal Component Analysis and Long Time Protein Dynamics. *J. Phys. Chem.* **1996**, *100*, 2567–2572. [CrossRef]
59. Maisuradze, G.G.; Liwo, A.; Scheraga, H.A. Principal Component Analysis for Protein Folding Dynamics. *J. Mol. Biol.* **2009**, *385*, 312–329. [CrossRef]
60. David, C.C.; Jacobs, D.J. Principal component analysis: A method for determining the essential dynamics of proteins. *Protein Dyn. Methods Protoc.* **2014**, *1084*, 193–226.
61. Bakan, A.; Meireles, L.M.; Bahar, I. ProDy: Protein dynamics inferred from theory and experiments. *Bioinformatics* **2011**, *27*, 1575–1577. [CrossRef]
62. Humphrey, W.; Dalke, A.; Schulten, K. VMD: Visual molecular dynamics. *J. Mol. Graph.* **1996**, *14*, 33–38. [CrossRef]

Disclaimer/Publisher's Note: The statements, opinions and data contained in all publications are solely those of the individual author(s) and contributor(s) and not of MDPI and/or the editor(s). MDPI and/or the editor(s) disclaim responsibility for any injury to people or property resulting from any ideas, methods, instructions or products referred to in the content.